Spectrally resolved wave-mixing between near- and far-infrared pulses in gas

2013 New J. Phys. 15 125011

(http://iopscience.iop.org/1367-2630/15/12/125011)

New Journal of Physics
The open access journal for physics

Spectrally resolved wave-mixing between near- and far-infrared pulses in gas

M Clerici[1,2,4], D Faccio[2], L Caspani[1], M Peccianti[1,3], O Yaakobi[1], B E Schmidt[1], M Shalaby[1], F Vidal[1], F Légaré[1], T Ozaki[1] and R Morandotti[1,4]

[1] INRS-EMT, 1650 Boulevard Lionel-Boulet, Varennes, Québec J3X 1S2, Canada
[2] School of Engineering and Physical Sciences, Heriot-Watt University, SUPA, Edinburgh EH14 4AS, UK
[3] Department of Physics and Astronomy, University of Sussex, Falmer, Brighton BN1 9QH, UK
E-mail: clerici@emt.inrs.ca and morandotti@emt.inrs.ca

New Journal of Physics **15** (2013) 125011 (13pp)
Received 7 May 2013
Published 9 December 2013
Online at http://www.njp.org/
doi:10.1088/1367-2630/15/12/125011

Abstract. We investigate the nonlinear wave-mixing in gases between intense, short optical pulses and long-wavelength fields (mid infrared and terahertz). We show numerically that the beating between the sum- and difference-frequency generation components can be isolated in the spectrogram of the interaction, and can be used to sample the electric field oscillations of the long-wavelength pulses. This, in turn, could be employed as a possible characterization method that provides information on the real electric field amplitude. Our numerical model is supported by spectrally resolved measurements of the four-wave mixing signals obtained from the interaction of intense, single-cycle terahertz fields ($\lambda > 15\,\mu$m) and optical pulses ($\lambda \simeq 800$ nm, 50 fs duration) in air.

[4] Authors to whom any correspondence should be addressed.

Contents

1. Introduction

Four-wave mixing (FWM) in gas media has been recently proposed and exploited for the detection of far-infrared broadband pulses [1]. By wave-mixing a near-infrared or visible short probe pulse with an unknown field in the less accessible mid- and far-infrared or terahertz (THz) spectral regions, the temporal profile of the latter can be mapped into a signal in the visible (or near-UV), where detection can be more easily performed. In typical conditions, the duration of the probe pulse is comparable to, or longer than, the duration of the investigated pulse. In this case, recording with a photodiode the up-converted signal as a function of the probe delay allows mapping the envelope of the unknown pulse (UP). On the other hand, if we wish to sample the electric field oscillation of the UP, a reference signal at the probe second harmonic has to be provided. This has been achieved by considering both supercontinuum components generated by the probe pulse itself [1] and heterodyne schemes where an external electric field is employed to bias the wave-mixing interaction [2].

Here we show that by spectrally resolving the radiation generated by FWM at wavelengths close to the second harmonic of the short, broad-bandwidth probe pulse, it is possible to isolate the beating signal between the sum- and difference-frequency components. Such a beating signal is an *electric*- (or THz-) *field induced second harmonic generation* (EFISH or TFISH, e.g. [3–6]), which arises as a consequence of a purely electronic, third order nonlinearity [7]. Differently from other mechanisms of mid-infrared induced second-harmonic generation relying on higher order, phononic-mediated interactions (see e.g. [8, 9]), EFISH can be regarded to as an instantaneous effect both in solids and in atomic gases, and hence maps the square of the instantaneous electric field of the investigated pulse.

In this paper we show that, within certain limitations, the time-resolved electric field of the pulse under test can be retrieved with a simple reconstruction procedure. Differently from other more standard approaches for the characterization of THz fields such as electro-optical sampling (EOS) [10–12] and air-biased coherent detection (ABCD) [2], and also in contrast to what can now be achieved by electric field streaking both at near- [13–15] and at far-infrared frequencies [16, 17], the proposed method does not allow the determination of the direction of the unknown electric field. Yet, we show that in the experimentally investigated case the retrieved information might be suitable for spectroscopic purposes.

2. Four-wave mixing of ultrashort pulses with long-wavelength fields in gases

We consider here FWM between a long-wavelength UP and a short, near-infrared or visible probe. We assume the nonlinear medium to be dispersion-less (both in the linear and nonlinear regimes, e.g. corresponding to a short propagation in gas) and the nonlinearity to be instantaneous (monoatomic gas). Although it is well known that delayed nonlinearities in air cannot in principle be neglected, the experimental results we shall present match well with this assumption, mostly due to the short, 50 fs probe pulse duration. Indeed, it has been shown that delayed nonlinearities (related e.g. to the excitation of roto-vibrational states in polyatomic gases) become important only for pulse durations longer than 80–100 fs [18–20]. For the case of monoatomic, e.g. noble, gases then only instantaneous nonlinearities are active under the additional assumption, satisfied in our experiments, that laser pulse intensities are such that only weak gas ionization occurs and any plasma nonlinearities are thus also negligible. Confirmation of this reasoning also comes from the fact that no qualitative difference was observed in our experiments when using nitrogen or argon gas.

Considering a variable delay τ between the two involved pulses we can write the polarization term associated with the medium nonlinear response as [7]

$$P_{\mathrm{NL}}(t,\tau) \propto \chi^{(3)}\left[E_{\mathrm{UP}}(t)+E_{\mathrm{p}}(t-\tau)\right]^3, \tag{1}$$

where $E_{\mathrm{p,UP}}$ are the probe and UP real fields, respectively. We consider the spectrogram of the nonlinear interaction, as recorded by a frequency-resolved slow detector, i.e.

$$I_{\mathrm{FWM}}(\tau,\omega) \propto \left|\int \mathrm{d}t \mathrm{e}^{\mathrm{i}\omega t} P_{\mathrm{NL}}(t,\tau)\right|^2, \tag{2}$$

where for the sake of simplicity, we dropped any additional frequency dependent term. If we limit our investigation to the up-frequency shifting processes (above the probe carrier), the spectrogram reduces to

$$I_{\mathrm{FWM}}(\tau,\omega) \propto \left|\int \mathrm{d}t \mathrm{e}^{\mathrm{i}\omega t} E_{\mathrm{UP}}(t) E_{\mathrm{p}}^2(t-\tau)\right|^2. \tag{3}$$

On the other hand, the result of a delay-resolved measurement performed via a slow device without spectral resolution, can be written as a cross-correlation

$$I_{\mathrm{FWM}}(\tau) \propto \int \mathrm{d}t \left|E_{\mathrm{UP}}(t) E_{\mathrm{p}}^2(t-\tau)\right|^2 \propto \int \mathrm{d}\omega I_{\mathrm{FWM}}(\tau,\omega), \tag{4}$$

where the last proportionality holds due to Parseval's theorem.

We now introduce a sampling width $\sigma_{\mathrm{s}} \equiv 2\pi/(2^{1/2}\omega_{\mathrm{UP}})$. For a transform limited UP, σ_{s} could be considered as the minimum pulse width of the probe required to sample the temporal oscillations of the UP electric field. We can then distinguish two regimes for the cross-correlation of pulses with very different carrier frequencies: probe duration larger than the UP period, i.e. $\sigma_{\mathrm{p}} \gg \sigma_{\mathrm{s}}$, or vice versa, UP period longer than the probe duration, i.e. $\sigma_{\mathrm{p}} = \sigma_{\mathrm{s}}$ (where σ_{p} denotes the FWHM of the probe Gaussian pulse).

To illustrate the effect of the probe pulse duration and the two sampling limits in the FWM process we show in figure 1 a numerical example, obtained by considering Gaussian (transform-limited) pulses (probe p and UP) with carrier wavelengths $\lambda_{\mathrm{p}} = 800\,\mathrm{nm}$ and $\lambda_{\mathrm{UP}} = 10\,\mu\mathrm{m}$, respectively (thus $\sigma_{\mathrm{s}} \simeq 23.6\,\mathrm{fs}$), and durations $\sigma_{\mathrm{UP}} = 100\,\mathrm{fs}$ and: (a) $\sigma_{\mathrm{p}} = 50\,\mathrm{fs}$, i.e. $\sigma_{\mathrm{p}} \gg \sigma_{\mathrm{s}}$

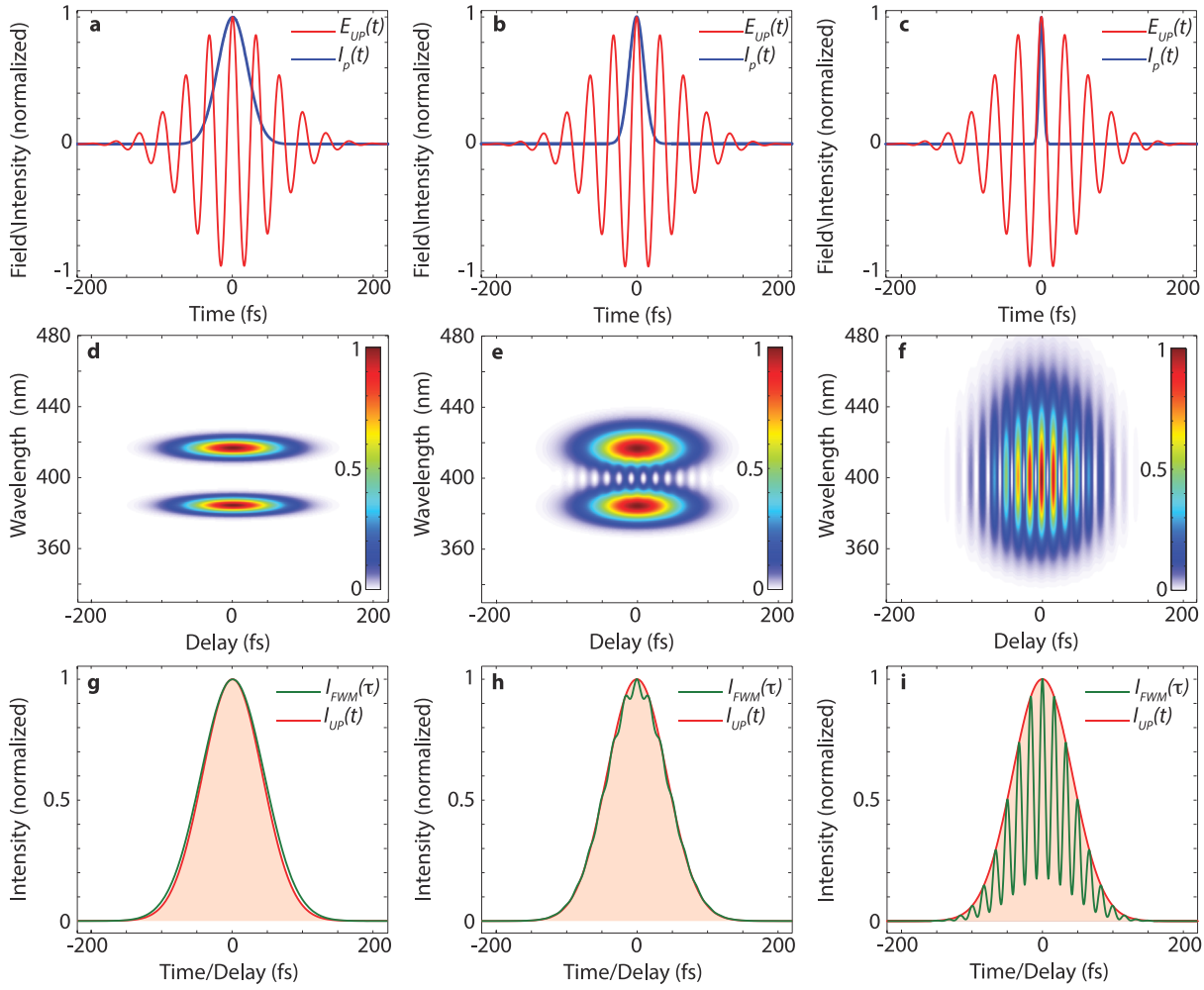

Figure 1. (a)–(c) Electric field temporal profiles (red) of the UP and intensities of the probe pulse (blue) for $\sigma_p = 50$ fs ($\sigma_p \gg \sigma_s$), 25 fs ($\sigma_p \simeq \sigma_s$) and 7.5 fs ($\sigma_p \ll \sigma_s$) durations, respectively. (d)–(f) Spectrograms (wavelength-resolved) for the three conditions above (a)–(c). (g)–(i) Delay-resolved intensity profile obtained by integrating the FWM spectrograms in (g)–(i) (green curves) compared with the UP intensity (red-shaded).

(left column in the figure); (b) $\sigma_p = 25$ fs, i.e. $\sigma_p \simeq \sigma_s$ (middle column) and finally (c) $\sigma_p = 7.5$ fs, i.e. $\sigma_p \ll \sigma_s$ (right column).

Figures 1(a)–(c) show the electric field $E_{UP}(t)$ overlapped with the probe pulse intensity $I_p(t)$ for the three cases considered above. In figures 1(d)–(f) we show the spectrograms $I(\tau, \lambda = 2\pi c/\omega)$ for the three cases (a)–(c). In the first case—left column, figures 1(a), (d), (g)—i.e. for $\sigma_p \gg \sigma_s$, two distinct contributions can be clearly observed, namely the sum- and difference-frequency generation (SFG and DFG, respectively) terms. These two terms indeed satisfy the energy conservation constraints:

$$\begin{aligned} &\text{SFG} : \omega_{\text{SFG}} = 2\omega_p + \omega_{\text{UP}}, \\ &\text{DFG} : \omega_{\text{DFG}} = 2\omega_p - \omega_{\text{UP}}. \end{aligned} \tag{5}$$

The cross-correlation, obtained according to (4), is presented for this case in figure 1(g) (green curve), and clearly does not show any field-dependent term, rather it maps the intensity of the UP (red-shaded curve).

Differently, for $\sigma_p \ll \sigma_s$—right column, figures 1(c), (f), (i)—the probe pulse samples the carrier oscillations of the UP and the spectrogram is clearly modulated at twice their frequency—see figure 1(f). This case is typically referred to as EFISH (or TFISH if the UP is a THz wave) and can be described considering the UP field as static (with respect to the probe field) and inducing an effective second order nonlinear process. In this case the nonlinear polarization may be simplified to

$$P_{NL}(t,\tau) \propto \chi^{(3)} E_{UP}(t) E_p^2(t-\tau) \propto \chi_{eff}^{(2)}(t) E_p^2(t-\tau), \tag{6}$$

where $\chi_{eff}^{(2)}(t) \equiv \chi^{(3)} E_{UP}(t)$, and the autocorrelation—figure 1(i)—results in a signal modulated as $E_{UP}^2(t)$. Yet, the modulation is characterized by limited visibility, as a consequence of the fact that the above relation truly holds for static fields only.

Finally, the condition for which the probe pulse duration is comparable to the carrier oscillation of the UP—central column, figure 1(b), i.e. for $\sigma_p \simeq \sigma_s$, is characterized by features common to the two above-mentioned regimes—see figure 1(e). In the spectrogram we clearly see the appearance of the SFG and DFG components, as well as of their beating in the region where their spectra overlap, i.e. at the frequency of the probe second harmonic (~400 nm in our example). Such beating maps the square of the UP instantaneous electric field and is a reminiscent signature of the EFISH effect. It should be noted however that no visible trace of the EFISH modulation would be recorded by the cross-correlation—see figure 1(h), green curve, which would still be proportional to the UP intensity profile.

Summarizing, for $\sigma_p \gg \sigma_s$ the FWM signal is characterized by two contributions, SFG and DFG, and the cross-correlation can map the UP intensity profile (for a probe *pulse* duration not significantly exceeding the UP one); for $\sigma_p \ll \sigma_s$ the FWM signal is modulated at twice the frequency of the UP electric field and this clearly appears in the cross-correlation signal (yet, the modulation is not completely visible). The case for $\sigma_p \simeq \sigma_s$ has features common to the two cases: the cross-correlation trace maps the UP intensity while a modulation proportional to $E_{UP}^2(t)$ appears in the spectrogram at frequencies close to the second harmonic of the probe, as a consequence of the beating of the SFG and DFG signals.

2.1. Field mapping

The modulation observed in the autocorrelation trace for $\sigma_p \ll \sigma_s$ carries information on the electric field trace of the UP, yet its reduced visibility prevents the proper extraction of such information. Increasing the visibility would require extremely short, not readily available optical probe pulses. For instance, in the numerical example considered in figure 1(c), a probe pulse of 7.5 fs is not short enough to fully resolve the 100 fs UP, as clearly shown by the limited visibility of the autocorrelation term, $I_{FWM}(\tau)$, in figure 1(i).

On the other hand, the modulation that appears in the spectrogram at the probe second harmonic wavelength for $\sigma_p \simeq \sigma_s$ (so that the sampling condition holds), has maximum visibility and can be employed for extracting relevant information on the UP electric field. Considering a lineout of the spectrogram we note that it maps the square of the instantaneous real electric field of the UP. In figure 2, the extracted, delay dependent curve (red) is

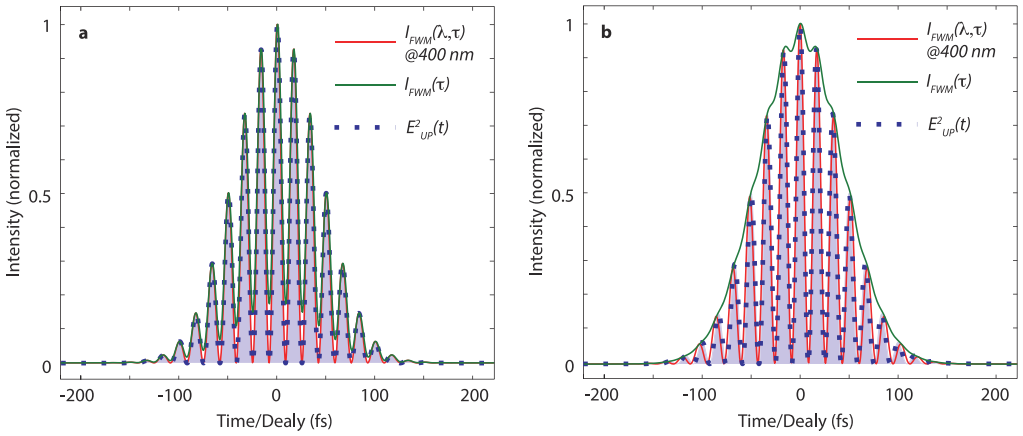

Figure 2. Comparison between the square of the electric field of UP (blue-dotted and shaded curve) and the expected results obtained (i) by recording the delay-dependent FWM signal (green curve) and (ii) by way of a lineout of the spectrogram at exactly the second harmonic wavelength (red curve) for (a) $\sigma_p = 7.5$ fs and (b) $\sigma_p = 25$ fs.

overlapped with $E^2_{UP}(t)$ (blue-dotted and shaded), both for $\sigma_p = 7.5$ fs—figure 2(a)—and $\sigma_p = 25$ fs—figure 2(b). For comparison, the green curve is the expected result of the cross-correlation—as in figures 1(h)–(i), green curve. Clearly, the visibility of the modulation is maximal in the spectrogram lineout, whereas it is limited in the cross-correlation signal also for very short probe pulses. Under proper conditions (see discussion below), a field reconstruction procedure can be employed to retrieve, from such a signal, the temporal electric field profile of the UP, with the exception of a global sign (i.e. the direction of the field cannot be determined). It is worth noting that this approach can be employed for the characterization of far-infrared but also of mid-infrared pulses. Indeed, thanks to available sources of ultrashort pulses with duration as short as a few femtoseconds, a lineout of the FWM spectrogram can provide relevant insight into the electric field of the UP with carrier wavelength as short as a few micrometres. In contrast to other phase-sensitive characterization techniques, e.g. SPIDER [21] and FROG [22], the proposed scheme is sensitive to the electric field and may thus provide a direct insight, e.g., into the carrier envelope phase of the UP and its spectral content (as shown below in our experimental case). For cases in which the direction of the electric field and its absolute strength (and not only a proportional signal) are required, more suitable, yet more experimentally demanding, techniques can be employed. Among those we can mention broadband EOS, ABCD and electric-field streaking. This last one has been employed, for instance, for the characterization of the electric field of pulses ranging from the near-infrared [13–15] to the THz [16, 17], yet it requires the detection of streaked electrons with equipment that is not readily available in all the laboratories dealing with ultrashort mid- and far-infrared pulses.

Finally, we note that when UPs with phase modulations are considered (e.g. not transform limited, as in the proposed examples), the sampling condition $\sigma_p \simeq \sigma_s$ refers to the highest instantaneous frequency of the UP, rather than to its carrier, and hence shorter probe pulses are required for larger bandwidth, phase modulated UPs.

2.2. *Unbalanced sum frequency generation and difference frequency generation*

The simplified case described so far relies on the assumption of equally efficient SFG and DFG. The finite size of the beams may however introduce an asymmetry in the process [7], which may in turn lead to a reduction in the visibility of the interference fringes. In this regard, it has been observed that even in a dispersion-less condition (e.g. a gas), when wave-mixing occurs between THz and optical beams, the SFG and DFG contributions are unbalanced due to spatial mode-matching (see e.g. [2, 23]). More specifically, Karpowicz and co-workers discussed the detection of THz pulses by ABCD in the condition that provides higher coherent signal, i.e. for THz and probe beams having the same Rayleigh length (R_{L}) [23, 24]. Under the assumption of Gaussian beams, they noted that the up-converted signals (both SFG and DFG) have beam widths close to that of the probe, but Gouy phases ϕ_{G} corresponding to different modes:

$$\begin{aligned}\phi_{\mathrm{G}}^{\mathrm{SFG}}(z) &= 2\phi_{\mathrm{G}}^{p}(z) + \phi_{\mathrm{G}}^{\mathrm{THz}}(z) \approx 3\phi_{\mathrm{G}}^{\mathrm{p}}(z),\\ \phi_{\mathrm{G}}^{\mathrm{DFG}}(z) &= 2\phi_{\mathrm{G}}^{p}(z) - \phi_{\mathrm{G}}^{\mathrm{THz}}(z) \approx \phi_{\mathrm{G}}^{\mathrm{p}}(z),\end{aligned} \tag{7}$$

where $R_{\mathrm{L,p}} = R_{\mathrm{L,THz}}$ is assumed. Hence, energy conversion in the SFG beam is strongly quenched (see also [24]) due to the large spatial, Gouy-phase mismatch. We note that the described imbalance is not a consequence of a multi-photon process and indeed it is not strictly dependent on the intensities of the involved pulses.

We study the impact of such effects on the field-dependent intensity oscillations that we are examining by introducing a parameter ε varying from -1 to $+1$ that modifies the relative weight of the DFG and SFG, such that

$$\frac{(1-\varepsilon)^2}{(1+\varepsilon)^2} = \frac{P_{\mathrm{DFG}}}{P_{\mathrm{SFG}}}, \tag{8}$$

where P indicates the related power. In this case, introducing the complex field $\mathcal{E}_{\mathrm{UP}}(t)$ such that $E_{\mathrm{UP}} = \mathrm{Re}[\mathcal{E}_{\mathrm{UP}}]$, we can re-write the FWM spectrogram as

$$I(\tau,\omega) \propto \left| \int \mathrm{d}t\, \mathrm{e}^{\mathrm{i}\omega t} \left[\left(\frac{1-\varepsilon}{2}\right) \mathcal{E}_{\mathrm{UP}}(t) + \left(\frac{1+\varepsilon}{2}\right) \mathcal{E}_{\mathrm{UP}}^{*}(t) \right] E_{\mathrm{p}}^{2}(t-\tau) \right|^2 . \tag{9}$$

The effect of such imbalance can be appreciated in figures 3(a)–(c), where we show the FWM spectrogram obtained considering a $\sigma_{\mathrm{UP}} = 100$ fs, 10 μm carrier wavelength, transform limited UP and a $\sigma_{\mathrm{p}} = 25$ fs probe at 800 nm, for three different imbalance conditions: $\varepsilon = 0.1$, 0.4 and 0.93, respectively (the spectrograms are shown in logarithmic scale). Although the beating signal decreases in amplitude for increasing imbalance, in the case of mild imbalance and depending on the sensitivity of the detector, it is still possible to retrieve relevant information on the UP electric field, performing a lineout of the spectrogram at the wavelength where the beating has maximum visibility. This is shown in figures 3(d)–(f), where the lineouts have been performed at $\lambda = 399.5$, 397.9 and 392.7 nm, respectively.

3. Experimental study

In order to validate our analysis, we have experimentally investigated the FWM spectrogram of an 800 nm pulse, delivered by a Ti:sapphire laser with a single-cycle broadband THz

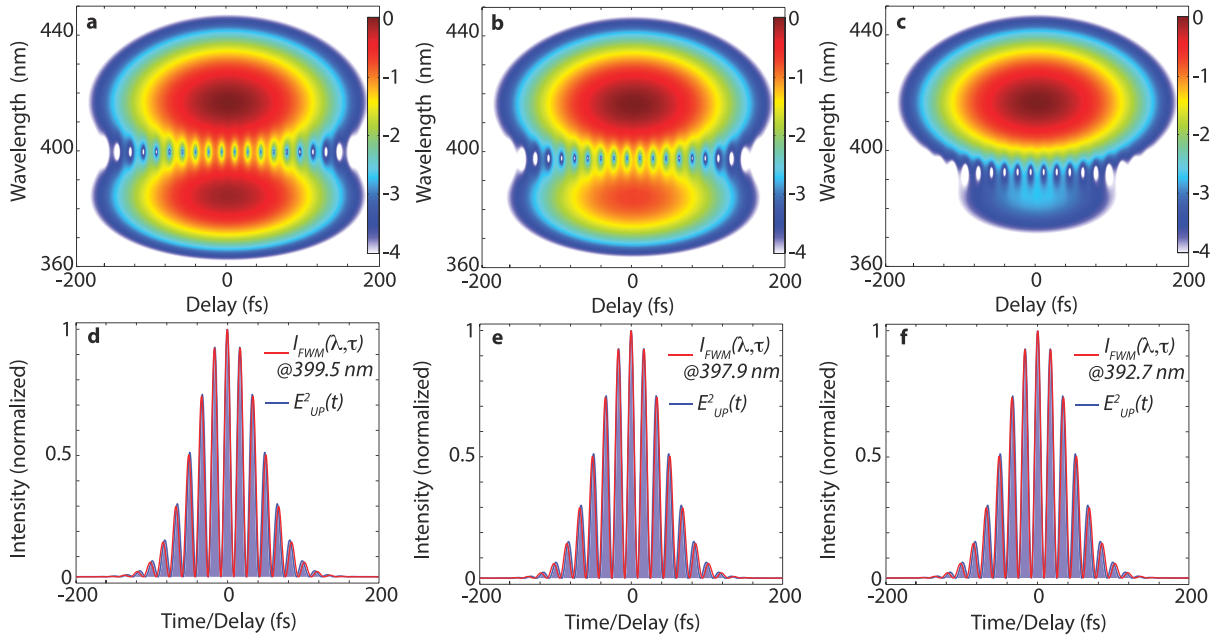

Figure 3. (a)–(c) FWM spectrogram in logarithmic scale (considering $\sigma_p \simeq \sigma_s$, see text for details) for different imbalance parameters: $\varepsilon = 0.1$, 0.4 and 0.93, respectively. (d)–(f) Lineout of the spectrogram at the wavelength where the beating has higher visibility (red curve). The lineout is compared to the square of the UP electric field profile (blue-shaded curve).

pulse generated by a two-colour air-plasma source [25–27], pumped by a mid-infrared laser [28, 29]. The experiments were performed at the 100 Hz beamline of the Advanced Laser Light Source. The THz pulses have been characterized by ABCD [2]. The ABCD was performed via a $\sigma_p = 50$ fs, 40 μJ probe pulse, applying a 27 kV cm^{-1} bias field to the region where the THz and the probe interact, and recording the signal with an amplified photodiode (*Femtowatt*, New-Focus). A scheme of the setup and the THz electric field trace measured via ABCD, along with its spectrum obtained by direct Fourier transform, are shown in figures 4(a)–(c), respectively.

Figure 4(a) depicts the setting employed for recording the spectrogram of the FWM. For this purpose, the external, bias static field has been removed and a spectrometer recording the signal at different probe-THz pulse delays has been inserted. In order to achieve high signal-to-noise ratio we employed an imaging spectrometer (*MS-260i*, Newport) coupled with a cooled charge coupled device (*620i*, QSI).

We recorded the spectrogram for different probe energies and beam sizes at the input of the focusing lens. In the investigated range of energies, spanning from 15 to 50 μJ, there are no relevant changes in the spectrogram. On the other hand, the input beam width strongly affects the spectrogram.

In figures 5(a)–(c) we show the recorded spectrograms for three different probe beam-widths: $\Delta_{x,p} = 5$, 8 and 10 mm, for an input energy $\simeq 30$ μJ. For small-aperture probe beams the spectrogram is rather asymmetric and no clear beating at the probe second harmonic wavelength could be detected. However, increasing the input beam-width leads to an increasingly visible beating signal.

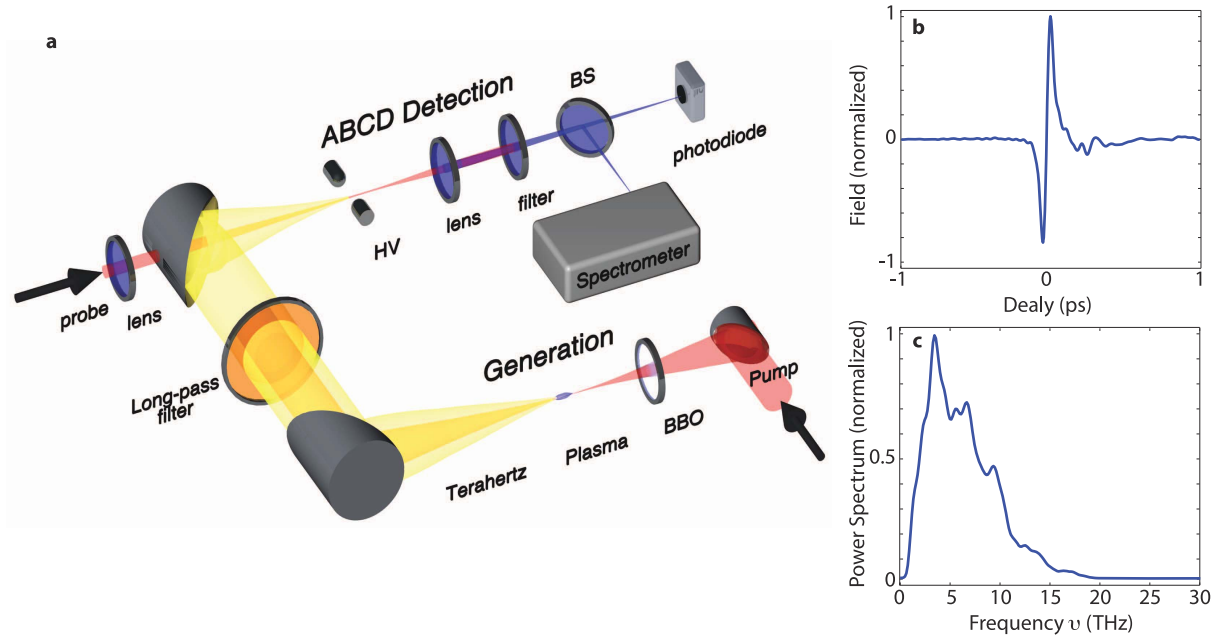

Figure 4. (a) Sketch of the experimental setup employed for the investigation of the FWM signal generated by overlapping THz pulses and optical probe fields (see text for details). Panels (b) and (c) are the THz electric field and spectrum recorded by ABCD.

This beating signal appears in the form of a single hole in our measurements due to the single cycle nature of the THz source. Pulses composed of more cycles would lead to an equivalent number of 'holes' in the spectrogram. We compare the experimentally recorded spectrogram with numerical simulations obtained by considering an input 50 fs duration probe pulse, centred at a wavelength of 795 nm, and the THz electric field trace recorded via ABCD. We adjust the imbalance parameter ε to graphically match the experimental spectrograms for the three beam-width conditions—figures 5(d)–(f); $\varepsilon = 1$, 0.8 and 0.5, respectively.

The first case—figures 5(a) and (d)—can be regarded as completely asymmetric process, i.e. where the SFG term, responsible for the shorter wavelength regions of the spectrogram, is completely suppressed. In this case no information on the THz electric field can be retrieved. The last case on the other hand—figures 5(c) and (f)—shows beating between the DFG and the suppressed SFG component, which can be employed for retrieving information on the THz instantaneous electric field.

As discussed above, the origin of the decreased imbalance between the efficiency of the SFG and DFG processes for increasing input probe beam-widths can be related to a decrease of the relative weight of the UP Gouy phase term in defining the emitted mode (the difference between $\phi_{\mathrm{G,UP}}(z)$ and $\phi_{\mathrm{G}}^{p}(z)$ decreases for decreasing probe Rayleigh lengths and thus also the difference between $\phi_{\mathrm{G}}^{\mathrm{SFG}}(z)$ and $\phi_{\mathrm{G}}^{\mathrm{DFG}}(z)$, see equation (7) for $\phi_{\mathrm{G}}^{\mathrm{THz}}(z) = \phi_{\mathrm{G,UP}}(z)$). Above, we have supposed a Gaussian UP, yet a different beam profile may result in a different Gouy phase, thus strongly affecting the imbalance. In order to investigate the effect of the beam profile on the output signal, we have measured the beam profile of the THz field emitted by two-colour ionization by means of a THz sensitive camera placed close to the focus of the parabolic telescope shown in figure 4(a). As expected, the THz emission is conical [30], yet with a very

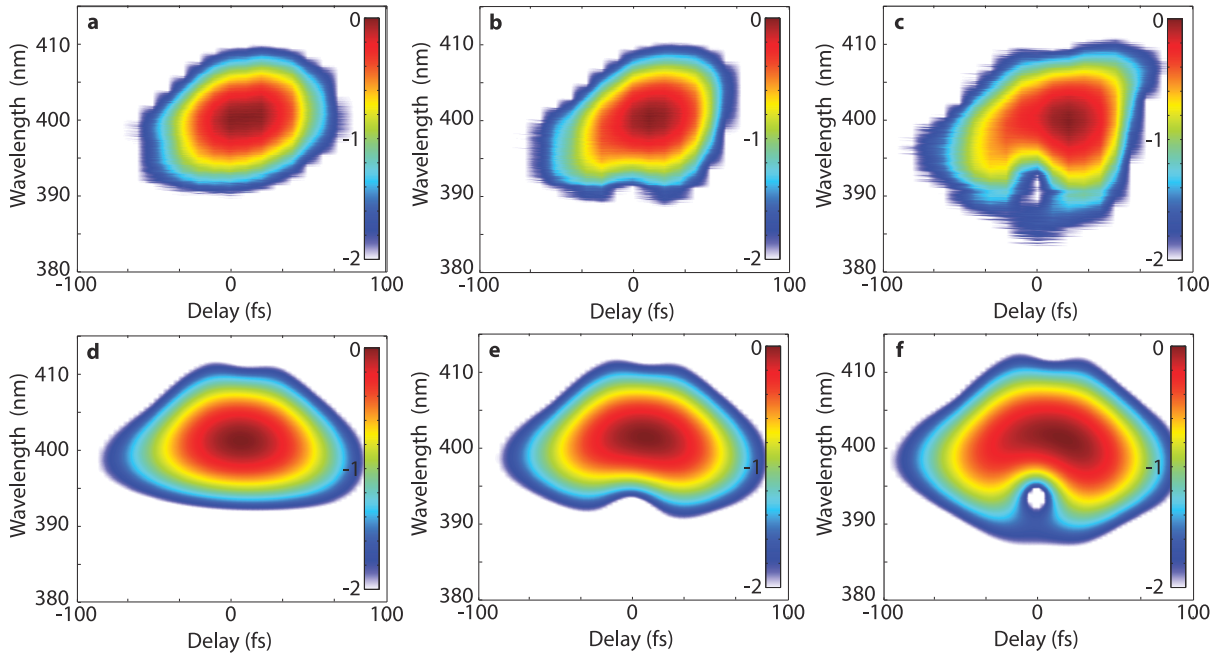

Figure 5. (a)–(c) Experimental FWM spectrograms (in logarithmic scale) recorded for increasing probe beam widths (5, 8 and 10 mm, respectively). Note the development of the beating at ∼393 nm. Panels (d)–(f) are numerical FWM spectrograms (in logarithmic scale) obtained considering the electric field trace recorded by ABCD and a 50 fs probe pulse duration. The imbalance term ε was adjusted to graphically match the experiments: 1, 0.8 and 0.5, respectively.

strong apodization. In order to further characterize the beam profile with higher resolution, we have performed a beam profile mapping exploiting the same TFISH process here investigated in gas, but in a diamond sample and employing collimated probe pulses [31]. This results in a THz beam profile that can be well fitted by a Bessel–Gauss function with a Gaussian width of the order of 80 μm. Due to this strong apodization, the conclusions based on a Gaussian beam hypothesis are therefore still valid. In order to verify the accuracy of the information on the UP retrieved by means of this method we performed a direct comparison with the electric field trace recorded by ABCD for the same relative position of the THz and the probe foci (so that the THz Gouy phase is the same in both the measurements [32–37]). In order to retrieve $E_{\mathrm{UP}}(t)$ from the value of $E^2_{\mathrm{UP}}(t)$ obtained from the spectrogram lineout we need to recover the information on the sign of $E_{\mathrm{UP}}(t)$, and thus we have to identify all its zeros. We first find all the local minima in $\sqrt{E^2_{\mathrm{UP}}(t)}$ and then all the local maxima in the absolute value of its first order derivative, $|\mathrm{d}\sqrt{E^2_{\mathrm{UP}}(t)}/\mathrm{d}t|/\sqrt{E^2_{\mathrm{UP}}(t)}$. We identify as zeros of $E_{\mathrm{UP}}(t)$ all the points that belong to both these sets, since we consider that a zero in a function results in a cusp on the function absolute value. Clearly, one of the weak points of this method is that the zeros of $E_{\mathrm{UP}}(t)$ that are also saddle points would not be correctly identified. Nevertheless, we assume that this possibility is rare enough.

Once we identify all the zeros, we can retrieve $E_{\mathrm{UP}}(t)$ by considering alternately $+\sqrt{E^2_{\mathrm{UP}}(t)}$ and $-\sqrt{E^2_{\mathrm{UP}}(t)}$ for each portion of field included between two consecutive zeros. In this way, supposing we correctly identify all the zeros, we can reconstruct the complete

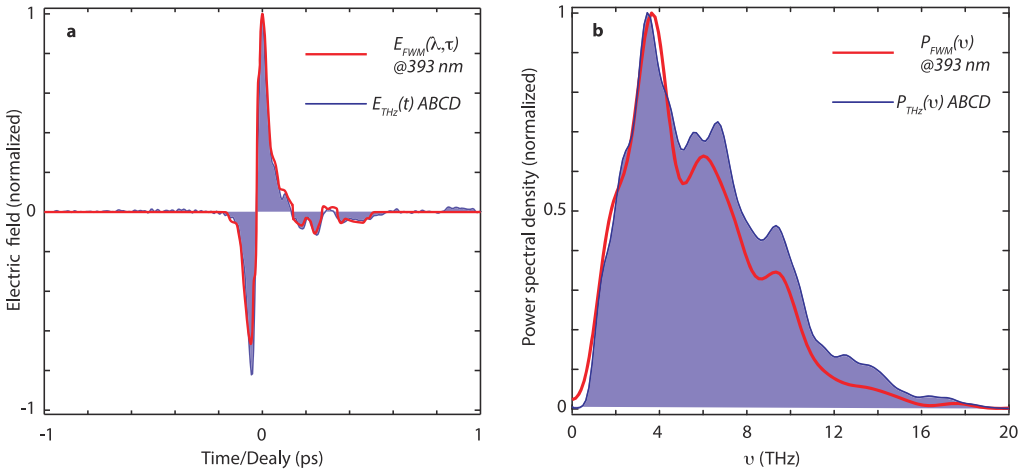

Figure 6. (a) Comparison between the retrieved signal from the lineout at 393 nm of the FWM spectrogram (red) and the THz electric field trace measured by ABCD detection (blue-shaded curve). In (b) the same comparison is performed for the power spectral density of the two signals.

field $E_{UP}(t)$, except for an overall sign, i.e. we may retrieve $-E_{UP}(t)$ instead of $E_{UP}(t)$. We further remark that this is not the case for other techniques like EOS, ABCD and streaking, which are able to map the electric field including the absolute sign (direction) and the field strength (when properly calibrated). In figure 6(a) the electric field trace obtained by ABCD detection (blue-shaded curve) is compared to the retrieved electric field trace obtained by a lineout at $\simeq 393$ nm of the FWM experimental spectrogram, once the field reconstruction procedure described above has been applied. We clearly see that the trace retrieved from the spectrogram lineout reproduces the ABCD measurement with only minor differences and can indeed provide an accurate mapping of the THz field. As further visual evidence, we evaluate the power spectral density for the retrieved trace and the ABCD THz field—see figure 6(b).

We finally note that the cross-correlation, performed, e.g., with a photodiode, for the FWM signal shown in figure 5(c) results in a signal that is proportional to the THz intensity profile, i.e. no modulations are observed as a function of the probe-THz pulse delay.

4. Conclusions

We have investigated the FWM between fields of very different wavelengths in dispersionless media (gases). We have shown that, depending on the ratio between the short wavelength pulse (probe) duration and the carrier oscillation period of the long wavelength field (UP), the nonlinear interaction results either in a signal that is proportional to the square of the instantaneous field of the UP, or to its intensity profile. In a condition where these two quantities are at least comparable, the field information for the UP can still be retrieved by a lineout of the interaction spectrogram at the wavelength where the beating between the involved SFG and DFG processes has maximum visibility. We showed that the beating maps the UP electric field profile and we discussed the case of unbalanced SFG and DFG. To validate our analysis we reported our measurement of the FWM spectrograms obtained considering a short, 800 nm probe pulse and a broadband THz field generated by air ionization. In this case we compared

the recorded THz field with the results of a reconstruction procedure that translates the beating signal into electric field information (with the exception of a global sign).

As a final remark, we note that the beating between unbalanced SFG and DFG has also been recently observed for THz pulses interacting with optical probe fields in bulk diamond samples [6].

Acknowledgments

MC acknowledges the support of the IOF People Programme (Marie Curie Actions) of the European Union's FP7-2012, KOHERENT, GA 299522. DF acknowledges financial support from the Engineering and Physical Sciences Research Council EPSRC, Grant EP/J00443X/1 and from the European Research Council under the European Union's Seventh Framework Programme (FP/2007-2013)/ERC Grant Agreement no. 306559. LC, OY and MS acknowledge the FQRNT (Fonds Québécois de la Recherche sur la Nature et les Technologies) MELS fellowship programme (Files 168739, 168900 and 140277, respectively). The research in Canada has been supported by NSERC (Natural Sciences and Engineering Research Council of Canada), FQRNT and MDEIE (Ministère du Développement Économique, de l'Innovation et de l'Exportation).

References

[1] Dai J, Xie X and Zhang X-C 2006 Detection of broadband terahertz waves with a laser-induced plasma in gases *Phys. Rev. Lett.* **97** 103903

[2] Karpowicz N *et al* 2008 Coherent heterodyne time-domain spectrometry covering the entire 'terahertz gap' *Appl. Phys. Lett.* **92** 011131

[3] Ohlhoff C, Meyer C, Lüpke G, Löffler T, Pfeifer T, Roskos H G and Kurz H 1996 Optical second-harmonic probe for silicon millimeter-wave circuits *Appl. Phys. Lett.* **68** 1699–701

[4] Nahata A and Heinz T F 1998 Detection of freely propagating terahertz radiation by use of optical second-harmonic generation *Opt. Lett.* **23** 67–9

[5] Cook D, Chen J, Morlino E A and Hochstrasser R M 1999 Terahertz-field-induced second-harmonic generation measurements of liquid dynamics *Chem. Phys. Lett.* **309** 221–8

[6] Clerici M, Caspani L, Rubino E, Peccianti M, Cassataro M, Busacca A, Ozaki T, Faccio D and Morandotti R 2013 Counterpropagating frequency mixing with terahertz waves in diamond *Opt. Lett.* **38** 178–80

[7] Boyd R W 2008 *Nonlinear Optics* (New York: Academic)

[8] Sahraoui B and Kityk I V 2003 Mid-infrared light-induced second-harmonic generation in specific glasses *J. Opt. A: Pure Appl. Opt.* **5** 174–9

[9] Kityk I V and Sahraoui B 2005 Phonon-assisted second harmonic generation in $As_{1-x}Bi_xTe_3$-$CaBr_2$-$PbBr_2$ glasses. *J. Phys. Chem.* B **109** 3163–8

[10] Valdmanis J A 1982 Picosecond electro-optic sampling system *Appl. Phys. Lett.* **41** 211–2

[11] Wu Q and Zhang X-C 1997 Free-space electro-optics sampling of mid-infrared pulses *Appl. Phys. Lett.* **71** 1285–6

[12] Gallot G and Grischkowsky D 1999 Electro-optic detection of terahertz radiation *J. Opt. Soc. Am.* B **16** 1204–12

[13] Itatani J, Quéré F, Yudin G, Ivanov M, Krausz F and Corkum P 2002 Attosecond streak camera *Phys. Rev. Lett.* **88** 173903

[14] Krausz F and Ivanov M 2009 Attosecond physics *Rev. Mod. Phys.* **81** 163–234

[15] Frühling U 2011 Light-field streaking for FELs *J. Phys. B: At. Mol. Opt. Phys.* **44** 243001

[16] Cavalleri A, Wall S, Simpson C, Statz E, Ward D W, Nelson K A, Rini M and Schoenlein R W 2006 Tracking the motion of charges in a terahertz light field by femtosecond x-ray diffraction *Nature* **442** 664–6
[17] Frühling U, Wieland M, Gensch M, Gebert T, Schütte B, Krikunova M, Kalms R, Budzyn F, Grimm O, Rossbach J, Plönjes E and Drescher M 2009 Single-shot terahertz-field-driven x-ray streak camera *Nature Photon.* **3** 523–8
[18] Varma S, Chen Y-H and Milchberg H 2008 Trapping and destruction of long-range high-intensity optical filaments by molecular quantum wakes in air *Phys. Rev. Lett.* **101** 205001
[19] Wahlstrand J K, Cheng Y-H, Chen Y-H and Milchberg H M 2011 Optical nonlinearity in Ar and N_2 near the ionization threshold *Phys. Rev. Lett.* **107** 103901
[20] Wahlstrand J K, Cheng Y-H and Milchberg H M 2012 Absolute measurement of the transient optical nonlinearity in N_2, O_2, N_2O, and Ar *Phys. Rev.* A **85** 043820
[21] Iaconis C and Walmsley I A 1998 Spectral phase interferometry for direct electric-field reconstruction of ultrashort optical pulses *Opt. Lett.* **23** 792–4
[22] Trebino R, DeLong K W, Fittinghoff D N, Sweetser J N, Krumbügel M A, Richman B A and Kane D J 1997 Measuring ultrashort laser pulses in the time-frequency domain using frequency-resolved optical gating *Rev. Sci. Instrum.* **68** 3277–95
[23] Lu X, Karpowicz N and Zhang X C 2009 Broadband terahertz detection with selected gases *J. Opt. Soc. Am.* B **26** A66–73
[24] Karpowicz N 2009 *Physics and Utilization of Terahertz Gas Photonics* (Troy, NY: Rensselaer Polytechnic Institute) http://search.proquest.com//docview/304984645
[25] Cook D J and Hochstrasser R M 2000 Intense terahertz pulses by four-wave rectification in air *Opt. Lett.* **25** 1210–2
[26] Thomson M D, Kreß M, Löffler T and Roskos H G 2007 Broadband THz emission from gas plasmas induced by femtosecond optical pulses: from fundamentals to applications *Laser Photonics Rev.* **1** 349–68
[27] Kim K-Y, Glownia J H, Taylor A J and Rodriguez G 2007 Terahertz emission from ultrafast ionizing air in symmetry-broken laser fields *Opt. Express* **15** 4577–84
[28] Clerici M *et al* 2013 Wavelength scaling of terahertz generation by gas ionization *Phys. Rev. Lett.* **110** 253901
[29] Schmidt B E, Shiner A D, Giguère M, Lassonde P, Trallero-Herrero C A, Kieffer J-C, Corkum P B, Villeneuve D M and Légaré F 2012 High harmonic generation with long-wavelength few-cycle laser pulses *J. Phys. B: At. Mol. Opt. Phys.* **45** 074008
[30] Liu J, Dai J and Zhang X C 2011 Ultrafast broadband terahertz waveform measurement utilizing ultraviolet plasma photoemission *J. Opt. Soc. Am.* B **28** 796–804
[31] Clerici M, Faccio D, Caspani L, Peccianti M, Rubino E, Razzari L, Légaré F, Ozaki T and Morandotti R 2013 CCD-based imaging and 3D space–time mapping of terahertz fields via Kerr frequency conversion *Opt. Lett.* **38** 1899–901
[32] Feng S, Winful H G and Hellwarth R W 1998 Gouy shift and temporal reshaping of focused single-cycle electromagnetic pulses *Opt. Lett.* **23** 385–7
[33] Ruffin A, Rudd J, Whitaker J, Feng S and Winful H 1999 Direct observation of the Gouy phase shift with single-cycle terahertz pulses *Phys. Rev. Lett.* **83** 3410–3
[34] Lindner F, Paulus G, Walther H, Baltuška A, Goulielmakis E, Lezius M and Krausz F 2004 Gouy phase shift for few-cycle laser pulses *Phys. Rev. Lett.* **92** 113001
[35] Lin Q, Zheng J, Dai J, Ho I and Zhang X-C 2010 Intrinsic chirp of single-cycle pulses *Phys. Rev.* A **81** 043821
[36] Zhang L, Zhong H, Mu K, Zhang C and Zhao Y 2012 Phase characterization in broadband THz wave detection through field-induced second harmonic generation *Opt. Express* **20** 75–80
[37] He H and Zhang X-C 2012 Analysis of Gouy phase shift for optimizing terahertz air-biased-coherent-detection *Appl. Phys. Lett.* **100** 061105